Dalton Transactions

Accepted Manuscript

ROYAL SOCIETY OF CHEMISTRY

www.rsc.org/dalton

Polyoxometalate-Based Complex with Visible-Light Photochromism as Electrocatalyst for Generating Hydrogen from Water

Yun Gong,* Yong Xi Yang, Miao Miao Zhang, Xiao Lin Gao, Jun Li Yin and Jian Hua Lin*

A polyoxometalate-based complex can act as the electrocatalyst for H_2 evolution reaction (HER) and the HER current is enhanced with visible-light irradiation.

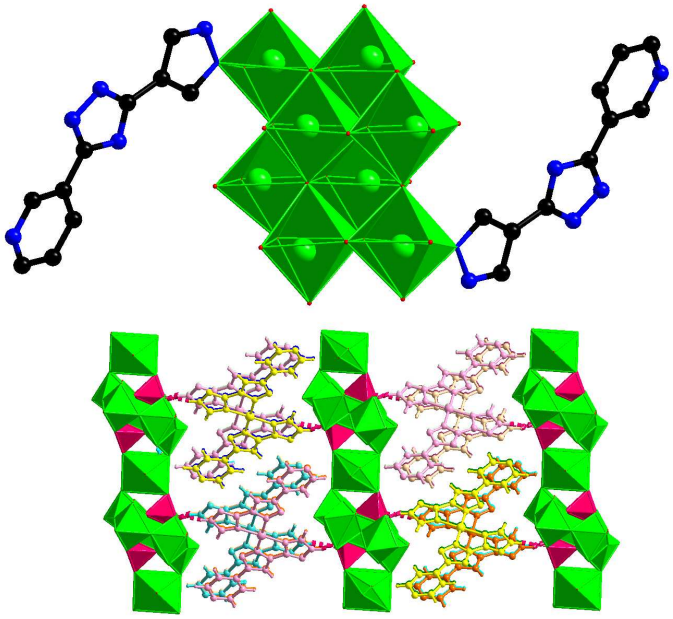

Polyoxometalate-based complex with visible-light photochromism as electrocatalyst for generating hydrogen from water

Yun Gong, [*,a] Yong Xi Yang, [a] Miao Miao Zhang,[a] Xiao Lin Gao, [a] Jun Li Yin [a] and Jian Hua Lin [*, a, b]

[a] *Department of Applied Chemistry, College of Chemistry and Chemical Engineering, Chongqing University, Chongqing 400030, P. R. China Tel: +86-023-65106150 E-mail: gongyun7211@cqu.edu.cn*

[b] *Zhejiang University, Hangzhou 310058, P. R. China Tel: +86-0571-88981583 E-mail: jhlin@zju.edu.cn; jhlin@cqu.edu.cn; jhlin@pku.edu.cn*

Two polyoxometalate (POM)-based complexes formulated as $(HL1)_2(Mo_8O_{26})\cdot 2HL1\cdot 11H_2O$ (L1 = 3- (5- (1H -pyrazol -4 -yl) -1H -1,2,4 –triazol -3 -yl) pyridine) (**1**) and $Co_2(L2)_4[P_2Mo^{VI}{}_5O_{23}Mo^{II}(H_2O)_2]\cdot 3H_2O$ (L2 = 4-(5-(2H-1,2,4-triazol-3 -yl) -2H -1,2,4 –triazol -3 -yl) pyridine) (**2**) have been synthesized and structurally characterized by single-crystal X-ray diffraction. Complex **1** shows a bi-capped POM with the two Mo centers from the $[Mo_8O_{26}]^{4-}$ moiety coordinated by two **HL1** ligands via two Mo-N bonds. Complex **2** consists of a mononuclear unsaturated coordinated Co(II) unit and $[P_2Mo^{VI}{}_5O_{23}Mo^{II}(H_2O)_2]^{4-}$ moiety, in which $[P_2Mo^{VI}{}_5O_{23}Mo^{II}(H_2O)_2]^{4-}$ shows a chain-like structure constructed by edge-sharing or vertice-sharing $\{MoO_6\}$ and $\{PO_4\}$ polyhedra. The two complexes are both soluble in neutral aqueous solution and they can electrocatalyze H_2 evolution reaction (HER) from water with lowered overpotentials and enhanced currents, and complex **1** shows better electrocatalytic activity for the HER than complex **2**. Complex **1** shows visible-light photochromism. And in the presence of complex **1**, the HER current is enhanced with visible-light irradiation in comparison to the current without light irradiation.

Introduction

Due to the current global energy crisis, scientists are devoted to explore renewable resources to meet the energy demands.[1] Hydrogen is an ideal energy carrier, the search for electrocatalyst that would allow facilitating the proton reduction to H_2 from water is now an area of great interest.[2,3] Platinum metal is an excellent catalyst for H_2 production, however, it is not a sustainable material for large-scale applications due to its limited reserves on Earth. Earth-abundant metal molecular catalysts which mimic the hydrogenase active sites have been investigated for electrochemical H_2 production over the last decade. [4]

Recently, our study has been mainly focused on the synthesis and characterization of novel metal complexes, which show rich structural features and electrocatalytic properties for H_2 evolution reaction (HER) from water.[5]

Polyoxometalates (POMs), as a unique class of metal-oxide clusters, have drawn increasing attention in recent years, due to their abundant structures, diverse properties and potential applications in catalytic activities, reversible redox behavior and photochromic or electrochromic responses.[6] However, POMs are rarely explored in the field of electrocatalyst so far for generating H_2 from water.[7]

Usually, POMs are not electroconductive, which limits their uses in electrochemical fields. Our strategy to solve the problem is to obtain the aqueous solutions of POMs, in which they show ionic conductivities. Based on the situation, herein, we synthesized two N-donating ligands, 3-(5-(1H-pyrazol-4-yl)-1H-1,2,4-triazol-3-yl)pyridine) (**L1**) and 4-(5-(2H-1,2,4-triazol-3-yl)-2H-1,2,4-triazol-3-yl)pyridine) (**L2**) (**Scheme 1**).[8] Neutral N donors in the ligands make it possible to introduce anionic POM into the structure of the metal complex. In the present work, two POM-based complexes formulated as $(HL1)_2(Mo_8O_{26})\cdot 2HL1\cdot 11H_2O$ (**1**) and $Co_2(L2)_4[P_2Mo^{VI}{}_5O_{23}Mo^{II}(H_2O)_2]\cdot 3H_2O$ (**2**) were in situ synthesized hydrothermally. Both of them are soluble in neutral aqueous solution. Their cyclic voltammograms (CVs), electrochemical impedance spectroscopies (EISs), controlled potential electrolysis (CPE) experiments, thermal stabilities and UV-Vis absorption spectra have been investigated. Complex **1** shows visible-light photochromism. The electrocatalytic properties of complex **1** towards the HER from water with and without visible-light irradiation have also been investigated.

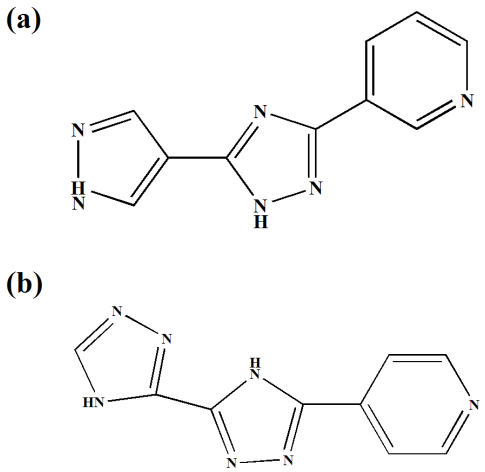

Scheme 1 Schematic representation of **L1 (a)** and **L2 (b)**.

Experimental

General Considerations

All chemicals purchased were of reagent grade and used without further purification. The melting point was determined using an uncorrected X-4 melting point apparatus of Beijing Kaifu Company. C, H, N elemental analyses were performed on an Elementar Vario MICRO E III analyzer. IR spectra were recorded as KBr pellets on a Nicolet iS50 FT-IR spectrometer. The powder XRD (PXRD) data were collected on a RIGAKU DMAX2500PC diffractometer using Cu Kα radiation. UV-Vis

spectra were measured on a HITACHI U-4100 UV-vis spectrophotometer. TGA was performed on a NETZSCH STA 449C thermogravimetric analyzer in flowing N_2 with a heating rate of 10°C·min^{-1}.

Electrochemical Measurements

A saturated calomel electrode (SCE), a platinum foil and a glassy carbon electrode (GCE) were used as the reference, counter and working electrode, respectively. The geometric area of the GCE is 0.2 cm^2. The measurements were recorded in 40 mL of N_2 degassed Na_2SO_4 (0.5 M) aqueous solution with or without 4mg complexes **1** or **2**, and a CHI660E electrochemical workstation was used for the electrochemical measurements. Before the electrochemical measurement, the working electrode was polished by abrasive paper and aluminum oxide, then ultrasonically washed by ethanol, acetone and distilled water. The amount of H_2 evolved was determined using gas chromatography (GC, 7890A, thermal conductivity detector (TCD), Ar carrier, Agilent). Electrochemical impedance spectroscopy (EIS) measurements were conducted on a CHI660E electrochemical workstation in the range of 0.01 Hz - 1 MHz.

Synthesis

Synthesis of L1: L1 was prepared according to the literature method.[8] Melting point: 158 ℃. IR (cm^{-1}): 3363(s), 2846(s), 2360(s), 1829(w), 1624(s), 1602(s), 1587(s), 1456(s), 1375(s), 1297(s), 1263(m), 1163(s), 1121(m), 1040(s), 1022(s), 990(m), 941(s), 881(m), 812(m), 754(s), 702(m), 634(w), 576(w), 441(w).

Synthesis of L2: L2 was prepared according to the literature method.[7] Melting point: ＞260 ℃. IR (cm^{-1}): 3382(s), 3108(s), 3008(s), 2862(s), 2802(s), 2648(s), 2501(s), 1883(s), 1614(s), 1482(w), 1428(s), 1346(s), 1299(m), 1272(s), 1218(m), 1171(w), 1089(s), 1035(s), 953(s), 872(s), 837(s), 751(m), 716(s), 642(m), 537(s).

Synthesis of $(HL1)_2(Mo_8O_{26})\cdot 2HL1\cdot 11H_2O$ (1): A mixture of **L1** (0.06 mmol, 0.013 g), MoO_3 (0.24 mmol, 0.035 g) and water (8 ml) was heated at 150 □ in Teflon-lined autoclaves for 3 days, then followed by slow cooling to room temperature. The resulting yellow block crystals were filtered off (yield: ca. 40 % based on **L1**). Elemental Anal. Found: C, 21.48; H, 2.60; N, 15.06 %. Calcd. for $C_{40}H_{58}Mo_8N_{24}O_{37}$: C, 21.50; H, 2.62; N, 15.04 %. IR (KBr, cm^{-1}): 3095(m), 1630(s), 1566(m), 1470(m), 1358(m), 1255(m), 1063(s), 993(m), 958(s), 912(s), 750(s), 677(s), 618(s), 556(s), 507(s).

Synthesis of $Co_2(L2)_4[P_2Mo^{VI}{}_5O_{23}Mo^{II}(H_2O)_2]\cdot 3H_2O$ (**2**): The synthesis of complex **2** was carried out as described above for complex **1**, but starting with the mixture of $Co(NO_3)_2\cdot 6H_2O$ (0.06 mmol, 0.017 g), **L2** (0.06 mmol, 0.013 g), MoO_3 (0.24 mmol, 0.035 g) and water (8 ml), and the initial mixture was adjusted to pH = 5 by H_3PO_4. After heated at 150 □ in Teflon-lined autoclaves for 3 days, the pH value of the final mixture was ca. 6-7. The yield of the grey block crystals is ca. 58 % based on **L2**. Elemental Anal. Found: C, 20.95; H, 1.82; N, 19.00 %. Calcd. for $Co_2C_{36}H_{38}N_{28}O_{28}P_2Mo_6$: C, 20.93; H, 1.85; N, 18.98 %. IR (KBr, cm^{-1}): 3451(s), 3105(s), 2860(s), 1637(s), 1514(m), 1469(m), 1444(m), 1419(m), 1347(m), 1302(m), 1265(m), 1234(m), 1210(m), 1105(s), 1060(s), 1023(s), 918(s), 835(m) , 750(m), 657(s), 541(s).

X-ray crystallography

Single-crystal X-ray data for the two complexes were collected on an Oxford XCalibur Eos diffractometer using graphite monochromated Cu K-alpha (λ = 1.54178 Å) radiation for complex **1** and Mo K-alpha (λ = 0.71073 Å) radiation for complex **2** at room temperature. Empirical absorption correction was applied. The structures were solved by direct methods and refined by the full-matrix least-squares methods on F^2 using the SHELXTL-97 software.[9] All non-hydrogen atoms were refined anisotropically. All of the hydrogen atoms were placed in the calculated positions. The crystal data and structure refinements for the two complexes are summarized in **Table 1**. Selected bond lengths and angles for the two complexes are listed in **Table S1** in the supporting information. The CCDC reference numbers are the following: 997898 for complex **1** and 997899 for complex **2**.

Table 1 Crystal data and structure refinements for complexes **1** – **2**

Complex	**1**	**2**
Empirical formula	$C_{40}H_{58}Mo_8N_{24}O_{37}$	$Co_2C_{36}H_{38}N_{28}O_{28}P_2Mo_6$
M	2234.62	2066.38
Crystal system	monoclinic	monoclinic
Space group	*C2/c*	*P2/c*
a /Å	29.9231 (13)	9.3047 (9)
b /Å	13.3754 (7)	9.5898 (9)
c /Å	19.4200 (8)	32.815 (3)
α /º	90	90
β /º	116.047 (4)	95.167 (9)
γ /º	90	90
V /Å^3	6983.1 (6)	2916.2 (5)
Z	4	2
D_{calcd}/g cm^{-3}	2.126	2.353
μ/mm^{-1}	12.363	1.971
No. of unique reflcns	6720	5135
reflcns used [$I > 2\acute{o}(I)$]	4991	3449
F(0 0 0)	4392	2020
Goodness-of-fit on F^2	1.061	1.038
Final R indices [$I>2\sigma(I)$]	R_1= 0.0420, wR_2= 0.1040	R_1= 0.0619, wR_2= 0.1207

$R_1=\Sigma||F_0|-|F_c||/\Sigma|F_0|$; $wR_2=\Sigma[w(F_0^2-F_C^2)^2]/\Sigma[w(F_0^2)^2]^{1/2}$

Results and discussion

Synthesis Complexes **1** and **2** were prepared by hydrothermal technique and the pH value of the reaction system was not of very crucial important for the crystallization of the aimed products. In the synthesis of the two complexes**,** the pH value of the final mixture can be maintained in the range of 6-7, indicating the two complexes are stable in neutral or weak acidic aqueous solution.

Crystal Structure of $(HL1)_2(Mo_8O_{26})\cdot 2HL1\cdot 11H_2O$ (1) Single-crystal X-ray diffraction analysis reveals that complex **1** crystallizes in the *monoclinic* space group *C2/c* (**Table 1**). In complex **1**, the asymmetric unit contains half $[Mo_8O_{26}]^{4-}$, one coordinated **HL1**, one uncoordinated **HL1** and 5.5 uncoordinated water molecules. In complex **1**, all the crystallographically independent Mo exhibit +6 oxidation state and possess octahedral coordination geometry [Mo-O 1.684 (6) - 2.431 (4) Å, Mo-N 2.243 (6) Å] (**Table S1**) Valences sum calculations show that all the molybdenum atoms are in the +6 oxidation state.[10] Complex **1** is a bi-capped polyoxometalate

with two **HL1** ligands coordinated to the two Mo centers of the $[Mo_8O_{26}]^{4-}$ moiety via two terminal pyrazol N atoms (**Fig. 1a**). The $[Mo_8O_{26}]^{4-}$ unit has C_i symmetry and is composed of six edge-sharing $\{MoO_6\}$ octahedra and two $\{MoO_5N\}$ octahedra and thus displays the characteristic γ-octamolybdate arrangement (**Fig. 1a**).[11a] The two crystallographically independent **HL1** ligands are almost planar molecules. The dihedral angles between two neighboring aromatic rings of the coordinated **HL1** are 5.1 and 8.2 º, respectively. As for the uncoordinated **HL1**, the dihedral angles are 4.3 and 5.3 º, respectively. The pyridine atoms of the coordinated and uncoordinated **HL1** ligands are protonated, which are involved in the strong H bond interactions in complex **1** (**Table 2**). Then in complex **1**, different $(HL1)_2(Mo_8O_{26})$ units are connected via strong H bonds (**Table 2**) and π-π stacking interactions into three-dimensional (3D) supramolecular architecture (**Table 3** and **Fig. 1b**).

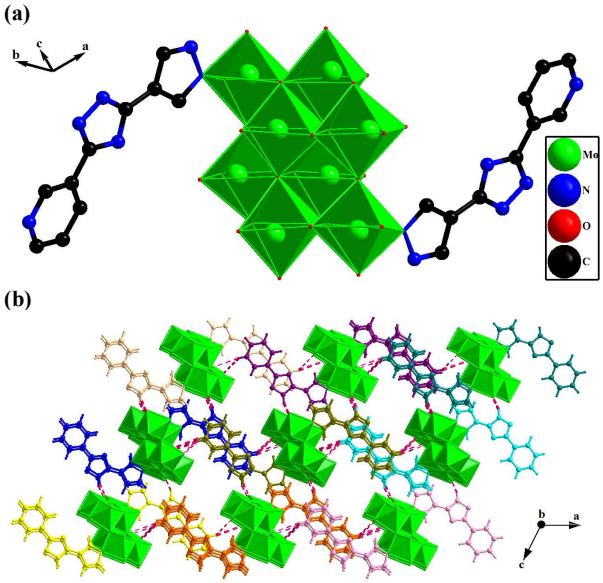

Fig.1. The $[Mo_8O_{26}]^{4-}$ moiety coordinated by two **HL1** ligands via two Mo-N bonds (H atoms omitted for clarity) (**a**); Strong H bonds and π-π stacking interactions are observed in complex **1** (H bonds denoted in pink dotted lines; the **HL1** ligands coordinated to different $[Mo_8O_{26}]^{4-}$ moieties denoted in different colors; uncoordinated water molecules omitted for clarity) (**b**).

Crystal Structure of $Co_2(L2)_4[P_2Mo^{VI}_5O_{23}Mo^{II}(H_2O)_2]\cdot 3H_2O$ (2) In an attempt get unsaturated coordination centers, Co(II) was introduced into the POM-based complex, complex **2** was obtained. Complex **2** crystallizes in the *monoclinic* space group *P2/c,* its asymmetric unit contains one Co(II), two **L2**, half $[P_2Mo^{VI}_5O_{23}Mo^{II}(H_2O)_2]^{4-}$ and 1.5 uncoordinated water molecules. One coordinated water molecule from the $[P_2Mo^{VI}_5O_{23}Mo^{II}(H_2O)_2]^{4-}$ is disordered over two locations (O15 and O15') and each site of them is half-occupied. In complex **2**, each P atom is in +5 oxidation state and shows a $\{PO_4\}$ tetrahedral coordination environment [P-O 1.513 (6) - 1.554 (6) Å]. In complex **2**, all the Mo atoms display $\{MoO_6\}$ octahedral coordination geometries. However, two terminal oxygen atoms of Mo (4) are from aqua ligands, which is different from the other Mo atoms, resulting in the Mo (4)-O distance [Mo (4)-O 2.256 (3) - 2.368 (6) Å] is longer than the average Mo-O length. Valences sum calculations show that Mo (4) is in the +2 oxidation state, and the other three crystallographically independent Mo (1), Mo (2) and Mo (3) are in the +6 oxidation states.[10] The $[P_2Mo^{VI}_5O_{23}Mo^{II}(H_2O)_2]^{4-}$ moiety is assembled into a one-dimensional (1D) chain by edge-sharing or vertice-sharing $\{MoO_6\}$ and $\{PO_4\}$ polyhedra (**Fig. 2a**). Co (1) exhibits a square-planar unsaturated coordination geometry, being coordinated by four triazol N atoms from two **L2** ligands [Co-N 1.946 (9) - 1.980 (9) Å], and valences sum calculations show that the crystallographically independent Co (1) is in the +2 oxidation state (**Fig. 2b** and **Table S1**).[10] The two crystallographically independent **L2** ligands in complex **2** both adopt a chelating coordination mode (**Fig. 2b**). Thus it is expected that the chelated Co (II) center is stable under electrocatalytic condition. The two **L2** ligands are almost planar molecules with 3.8, 7.5, 4.1 and 12.7 º of the dihedral angles between two neighboring aromatic rings. Strong H bonds (**Table 2**) and π-π stacking interactions (**Table 3**) are also observed in complex **2**, and complex **2** shows a 3D supramolecular architecture (**Fig. 2b**).

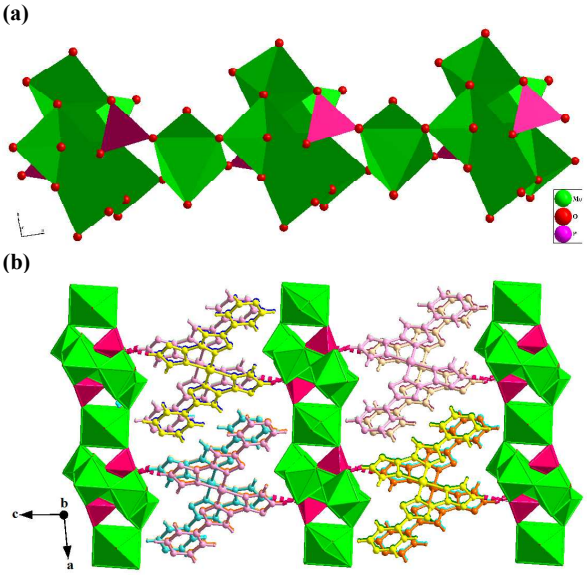

Fig.2. 1D $[P_2Mo^{VI}_5O_{23}Mo^{II}(H_2O)_2]_\infty$ chain in complex **2** (H atoms of the coordinated water molecules omitted for clarity) (**a**); 3D supramolecular architecture constructed by strong H bonds and π-π stacking interactions in complex **2** (uncoordinated water molecules and H atoms of the coordinated water molecules omitted for clarity; different Co units denoted in different colors; and H bonds denoted in pink dotted lines) (**b**).

UV-Vis absorption spectra The phase purities of complexes **1** and **2** were supported by the powder X-ray diffraction (PXRD) pattern of the bulk samples, which are consistent with the calculated patterns (**Fig. S1**). The UV-Vis absorption spectra of the free organic ligand and the bulk samples of the two complexes at room temperature are shown in **Fig. S2**. As shown in **Fig. S2**, **L1** displays absorption in the range of 230-800 nm with one intense peak at 284 nm and one weak shoulder peak at 580 nm. **L2** shows absorption in the range of 230-600 nm with two maxima at 255, 285 and 340 nm. They may be ascribed to the intraligand (n-π*or π-π*) transitions (ILCT).[12]

Complex **1** exhibits intense absorption in the range of 230-600 nm with two strong characteristic absorption bands of $[Mo_8O_{26}]^{4-}$ at 280 and 330 nm, and complex **2** shows absorption in the similar range with characteristic peaks of $[P_2Mo_6O_{25}]^{4-}$ at 280 and 315 nm, which are ascribed to the $O_d \rightarrow Mo$ and $O_{b,c} \rightarrow Mo$ charge-transfer transition bands, respectively.[13] And the absorption in the region of 600-800 nm for complex **2** may ascribe to the visible *d-d* transition.

Photochromic Property The diffuse reflectance spectra of the samples are shown in **Fig. S3**. According to the plot of the reflectance versus the radiation energy, the band gap of complexes **1-2** are calculated as 2.8 and 3.0 eV, respectively (The band-gap extraction method was elaborated in the

supporting information).[14] It is expected that complex **1** is photosensitive if exposed to visible light (λ > 400 nm).[15] Herein, a 300 W CEL-HXF300 Xe lamp from Zhong Jiao Jin Yuan company was used as the light source for visible-light photochromic experiment. The distance between the lamp and the sample was 5 cm.

(a)

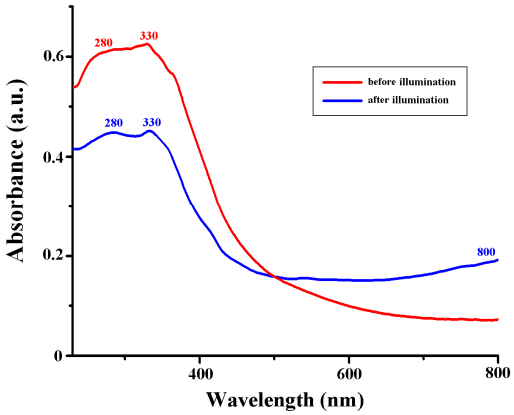

(b)

Fig.3 UV-vis absorption spectra (**a**) and photochromism images at room temperature for complex **1** (**b**) before (left) and after visible-light illumination (λ > 400 nm) (right).

Typical UV-visible absorption spectra of complex **1** before and after visible-light irradiation (λ > 400 nm) are shown in **Fig. 3a**. As described above, before visible-light irradiation, there are two O→Mo absorption bands for complex **1**. After visible-light irradiation for 4 h, the yellow crystals of complex **1** turn green (**Fig. 3b**). Meanwhile, it is found the O→Mo charge-transfer transition bands in the UV-vis spectrum showed no evident changes in position, but a large decrease in intensity. However, after irradiation, the sample displayed a new absorption band in the 600-800 nm of visible region (**Fig. 3b**), which is probably attributed to the metal-to-metal intervalence charge transfer (IVCT, $Mo^{V}\rightarrow Mo^{VI}$) band. [16a-c] The mechanism maybe involve the absorption of photons by the $[Mo_8O_{26}]^{4-}$, resulting in the generation of an electron-hole pair, then the Mo^{VI} atoms of the polyanions are reduced to form mixed-valence compound, leading to the observed photochromism.[16a-c] As described above, strong N-H···O hydrogen bonds are observed between the organic component and polyanions in complex **1** (**Table 2**), which also accounts for the photochromism of the sample in the solid state.[16d-e] And similar phenonmenon is observed in the Na_2SO_4 aqueous solution of complex **1** before and after visible-light illumination (λ > 400 nm). The solution of complex **1** shows UV absorption peaks at 230 and 270 nm before and after irradiation, which might be the O→Mo absorption bands. After visible-light illumination for 4 h, a new visible absorption band in the range of 400-800 nm appeared (**Fig. S4**).

Electrochemical Property of Complex 1 The redox property of complex **1** was evaluated by cyclic voltammetry (CV) experiment in a three-electrode cell with a GCE, SCE and platinum foil used as the working, reference and counter electrode, respectively. And the GCE has been polished and washed completely before measurement. In a 0.5 M Na_2SO_4 aqueous solution (40 mL), the bare GCE displays irreversible peaks at -0.55, -0.41 and + 0.78 V vs SCE in the potential range from -2.2 to +2.2 V at a scan rate of 0.01 $V\cdot s^{-1}$ (**Fig. 4** and **Fig. S5**), it is probably related with the impurity of the bare GCE though the GCE has been polished and washed completely. An irreversible peak at -1.75 V vs SCE was observed at the bare GCE (**Fig. 4** and **Fig. S5**), which coincides with the generation of bubbles, corresponding to the H_2 evolution reaction (HER) from neutral water. As we know, the theoretical potential for the HER in a neutral aqueous solution (pH = 7) on a clean Pt electrode is - 0.64 V vs SCE,[7a] indicating the overpotential for the HER in the blank system is -1.11 V vs SCE. In comparison, when 4 mg L1 was dissolved in the Na_2SO_4 solution (40 mL), two irreversible waves appeared at -0.68 and +0.74 V vs SCE at 0.01 $V\cdot s^{-1}$, similarly, which are probably ascribed to the redox of the impurity from the GCE. The reduction waves at the -0.26 and +1.18 V vs SCE in the CV are expected to be related with the redox of the π electrons from the aromatic rings of the ligand L1 (**Fig. 4, Fig. S5** and **Fig. S6**).[5] The CVs reveal the reduction potential of H^+ appeared at -1.75 V vs SCE in the presence of the ligand (**Fig. 4, Fig. S5** and **Fig. S6**), which is almost the same as that in the blank system, indicating the ligand L1 can't catalyze the HER.

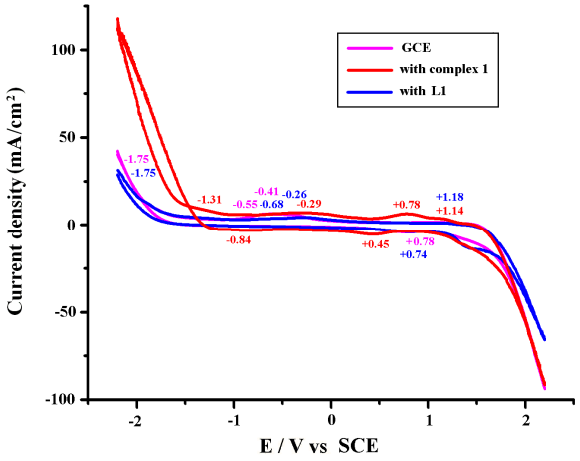

Fig. 4 CVs of the bare GCE in the 0.5 M Na_2SO_4 aqueous solution (40 mL) at a scan rate of 0.01 $V\cdot s^{-1}$ in the absence (pink) and presence of 4 mg L1 (blue) or 4 mg complex **1** (red).

In a parallel experiment, 4 mg complex **1** was dissolved in the 0.5 M Na_2SO_4 solution (40 mL), the CV at 0.01 $V\cdot s^{-1}$ shows more favorable electrochemical response with irreversible reduction waves at -0.29 and +1.14 V vs SCE, which are probably assigned to the redox of the π electrons from the ligand in complex **1** (**Fig. 4**).[5] The quasi-reversible couple (E_{pc} = + 0.78 V/E_{pa} = + 0.45 V) and the irreversible oxidation wave at - 0.84 V vs SCE may be related with the redox of Mo in the polyanions (**Fig. 4**).[17] In the presence of complex **1**, the onset potential for H^+ reduction is positively shifted to -1.31 V vs SCE (overpotential η = -0.67 V) at 0.01 $V\cdot s^{-1}$, and higher current for the HER are obtained with respect to the blank solution (**Fig. 4, Fig. S5** and **Fig. S7**), indicating complex **1** can catalyze the production of H_2.[5,18] It is expected that the reduction potential for

the HER is overlapped by the reduction of Mo(V) in complex **1**.[5a, 17] The Tafel curves in the absence and presence of complex **1** are shown **Fig. S8**, much lower HER overpotentials and much enhanced HER currents are observed in the presence of complex **1** than in the blank system. As we know, $\eta = a + b$ lgi, $a = -\{(2.303RT)/(\alpha nF)\}$lg i_0 , $b = \{(2.303RT)/(\alpha nF)\}$.[19] As shown in **Fig. S8b**, in the presence of complex **1**, it can be calculated the slope b = 1.695 and the intercept lg i_0= -3.17, then the charge-transfer efficiency α = 0.0174 and the exchanging current i_0 = 6.76×10^{-4} A.

In our case, the HER current density is in the magnitude of mA· cm^{-2} in the presence of complex **1**, which is much larger than the values reported in the literatures.[5,7a] It is probably due to the solubility of the complex in aqueous solution, which can afford ion conductivity in the system. In the aqueous solution, complex **1** can be dissociated into $[(HL1)_2(Mo_8O_{26})]^{2-}$ and $[HL1]^+$. After visible-light illumination, it is expected a new specie $[(HL1)_2(Mo_8O_{26})]^{n-}$ (n < 2) will be generated in the solution due to the partial reduction of Mo(VI).

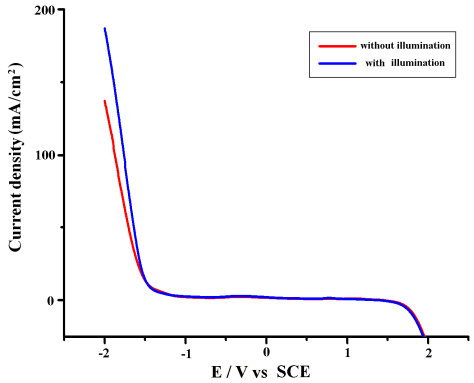

Fig. 5 Linear sweep voltammetry of the bare GCE in the 0.5M Na_2SO_4 aqueous solution (40 mL) at a scan rate of 0.005 V·s^{-1} in the presence of 4 mg complex **1** with and without visible-light illumination (λ > 400 nm).

As described above, complex **1** shows photochromic property. When complex **1** is irradiated by visible-light (λ > 400 nm), Mo (VI) can be partially reduced to Mo (V). As expected, if the reduction of H^+ is overlapped by the reduction of Mo (V), it is estimated that under visible-light irradiation, complex **1** can show enhanced electrocatalytic activity for the HER. As shown in **Fig. 5**, the linear sweep voltammetry (LSV) experiments reveal the HER current is enhanced in the presence of complex **1** under the visible-light illumination (λ > 400 nm), which proves our estimation that the reduction current for the HER is associated with reduction of the Mo (V) in complex **1**.

Controlled potential electrolysis (CPE) experiment over 0.5 h at - 1.4 V vs SCE (η = - 0.76 V and current density = 9.9 mA/cm^2) also proves the electrocatalytic activity of complex **1** for the HER. As depicted in **Fig. S9**, the GCE shows more favorable electrochemical responses in the presence of complex **1** than in the blank system under similar condition (η = - 0.76 V and current density = 4.0 mA/cm^2) with a turnover number (TON) of 0.3 mol of H_2 per mole of catalyst and 98 % Faradaic efficiency. Moreover, higher charge build-up is observed under the visible-light illumination than that without the illumination, indicating visible-light illumination can prompt the HER in the presence of complex **1** (**Fig. S9**).

The electrocatalytic mechanism of the complex is explained by the electrochemical impedance spectroscopy (EIS).[20] **Fig. 6** shows the Bode plots of the bare **GCE** in the absence and presence of complex **1** at -1.4 V. As shown in the Bode plots (**Fig. 6**), the R_s (electrolyte resistance) and R_{ct} (charge-transfer resistance) can be observed from the magnitude plot in the high and low frequency regions, respectively.[20] According to the Bode plots, the R_{ct} value for the HER in the presence of complex **1** is lower than that in the blank system, indicating the charge transfer is promoted in the presence of complex **1**, thus the current is enhanced in the presence of complex **1**.[20] Similarly, it is also found the R_{ct} value for the HER in the presence of complex **1** under the visible light irradiation (λ > 400 nm) is lower than that without the light irradiation, then the HER current is enhanced under the visible-light illumination in the LSV experiment.

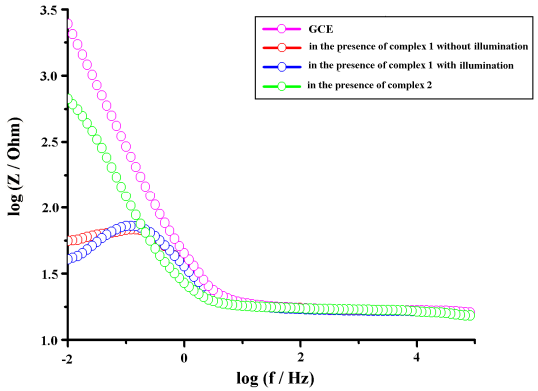

Fig.6 Bode plots (log of impedance magnitude vs. log f) at the initial potentials of -1.4 V in the absence and presence of complexes **1** or **2** with and without visible-light illumination (λ > 400 nm).

During the CV and electrolysis experiments, the pH value of the Na_2SO_4 solutions are in the range of 6-7, then complex **1** is stable in the neutral or weak acidic condition. As shown in **Fig. S10**, when the potential range is maintained at -2.2 to 2.2 V vs SCE, the HER peak currents can be almost kept over dozens of cycles. The electrochemical behavior in the presence of complex **1** is due to the $[Mo_8O_{26}]^{4-}$ moiety in complex **1**, which is a superior electron reservoir and it possesses superior redox property. The UV-vis spectra of the complex in Na_2SO_4 solution after CV cycles also demonstrate the stability of complex **1**. As shown in **Fig. S11**, after CV cycles, the solution of complex **1** shows similar UV absorption bands to the solution of complex **1** without electrochemical performance.

Electrochemical Property of Complex 2 The electrocatalytic activity of complex **2** for the HER was also evaluated under similar condition. As shown in **Fig. 7** and **Fig. S12**, when 4 mg complex **2** was dissolved in 0.5 M Na_2SO_4 solution (40 mL), the bare GCE exhibits electrochemical response with proton reduction at an onset potential of approximately -1.62 V vs SCE (overpotential η = -0.98 V) at 0.01 V·s^{-1}, which was positively shifted with respect to the blank solution (-1.75 V vs SCE, overpotential η = -1.11 V) with slightly enhanced current (**Fig. 7** and **Fig. S12**), indicating complex **2** can also act as an electrocatalyst for the HER. As shown in **Figs. S12-S13**, the irreversible reduction waves at -0.67 and +1.12 V vs SCE in the presence of complex **2** are similar to the redox waves at -0.55 and +1.18 V vs SCE in the presence of L2, indicating they are probably assigned to the redox of the π electrons from the ligand in complex **2**.[5] The irreversible redox waves at -0.91 and + 0.47 V vs SCE are probably associate with the redox of Mo atom in complex **2** (**Fig. 7** and **Fig. S12**).[17]

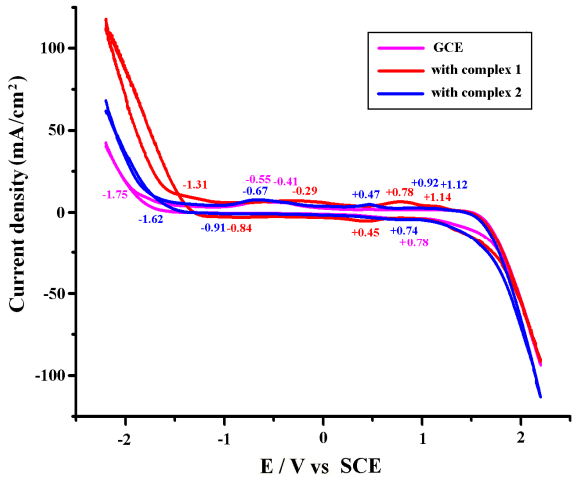

Fig. 7 CVs of the bare GCE in the 0.5 M Na_2SO_4 aqueous solution (40 mL) at a scan rate of 0.01 $V \cdot s^{-1}$ in the absence (pink) and presence of 4 mg complex **1** (red) or complex **2** (blue).

As shown in **Fig. 7**, the reduction overpotential of H^+ in the presence of complex **1** (- 0.67 V) is more positive than the - 0.98 V of overpotential in the presence of complex **2**, indicating complex **1** shows better electrocatalytic activity than complex **2**. The result is also proved by the Tafel plots of the two complexes, as shown in **Fig. S8**. As shown in **Fig. S8b**, in the presence of complex **2**, it is calculated that $log\ i_0$ = -3.41, b = 1.779, and the charge-transfer efficiency α = 0.0166 and the exchanging current $i_0 = 3.89 \times 10^{-4}$ A. The better electrocatalytic activity of complex **1** can be explained by the EIS. As shown in **Fig. 6**, Bode plot shows the R_{ct} value for the HER in the presence of complex **1** is lower than that in the presence of complex **2**, indicating the charge transfer is promoted by complex **1** more than by complex **2**.[20]

As shown in **Fig. S9**, 0.5h-CPE experiment at - 1.4 V vs SCE (η = -0.76V and current density = 5.2 mA/cm^2) shows the electrocatalytic activity of complex **2** for the HER with the Faradaic efficiency of 97 % and TON of 0.16 mol of H_2 per mole of complex **2**.

The electrochemical stability of complex **2** can be proved by the continuous CV experiment and the UV-vis spectra. As shown in **Fig. S14**, in the presence of complex **2**, the HER peak currents can be almost kept over dozens of CV cycles. And the solution of complex **2** shows similar UV absorption peaks at 230 and 260 nm before and after CV cycles, as shown in **Fig. S15**. Herein, though complex **2** is soluble in the electrolyte solution, the concentration of Co^{2+} in the solution is very low due to the chelating coordination of L2. According to the Nernst equation, $E\ (Co^{2+}/\ Co) = E^{\theta}\ (Co^{2+}/\ Co) + (0.0592/2)\ log\ C\ (Co^{2+})$, with the decrease of the concentration of Co^{2+} in the solution, E (Co^{2+}/Co) is decreased. Herein, E (Co^{2+}/Co) can be less than E (H^+/H_2), and Co^{2+} can be reduced into Co after the HER. Then complex **2** is stable under the electrochemical condition.

In the presence of complex **2**, the HER current density is also in the magnitude of $mA \cdot cm^{-2}$, which is due to the solubility of the complex in aqueous solution. In the aqueous solution, complex **2** can be dissociated into $[P_2Mo^{VI}_5O_{23}Mo^{II}(H_2O)_2]^{4-}$ and $[Co_2(L2)_4]^{4+}$. However, complex **1** possesses low overpotential and better electrocatalytic activity than complex **2**. As described above, complex **1** is constructed by L1 and $[Mo_8O_{26}]^{4-}$, and complex **2** consists of Co (II), L2 and $[P_2Mo^{VI}_5O_{23}Mo^{II}(H_2O)_2]^{4-}$. Unsaturated coordinated Co (II) center is observed in complex **2**, and complex **1** doesn't possess unsaturated metal center. The present work indicates it is probably that the overpotentials and electrocatalytic activities of the two complexes are not completely related with the unsaturated metal centers in the structures.[21] Herein, it is expected that the redox of Mo (V) is overlapped by the redox for the HER. The detailed mechanism is under investigation.

Thermal Stabilities of Complexes 1 and 2 In order to examine the thermal stabilities of complexes **1** and **2**, thermogravimetric analyses (TGAs) were carried out. The samples were heated up to 750 °C in N_2. As shown in **Fig. S16**, complex **1** shows a one step weight loss of 8.7 % in the range of 30-180 °C corresponding to the loss of the uncoordianted water molecules (calc. 8.9 wt %). And complex **2** releases its uncoordinated water molecules in the range of 30-170 °C with a loss of 2.0 wt % (calc. 1.8 wt %) (**Fig. S16**).

Conclusion

In conclusion, two complexes based on POMs formulated as $(HL1)_2(Mo_8O_{26})\cdot 2HL1\cdot 11H_2O$ (**1**) and $Co_2(L2)_4[P_2Mo^{VI}_5O_{23}Mo^{II}(H_2O)_2]\cdot 3H_2O$ (**2**) have been synthesized and structurally characterized by single-crystal X-ray diffraction. Complex **1** is a bi-capped POM with two Mo centers from the $[Mo_8O_{26}]^{4-}$ moiety coordinated by two **HL1** ligands via two Mo-N bonds. Complex **2** consists of a mononuclear unsaturated Co(II) unit and $[P_2Mo^{VI}_5O_{23}Mo^{II}(H_2O)_2]^{4-}$ moiety, in which $[P_2Mo^{VI}_5O_{23}Mo^{II}(H_2O)_2]^{4-}$ shows a 1D chain structure constructed by edge-sharing or vertice-sharing $\{MoO_6\}$ and $\{PO_4\}$ polyhedra. The two complexes are both soluble in neutral aqueous solution and they exhibit electrocatalytic activities toward generating H_2 from water with lowered overpotentials and enhanced currents, and complex **1** exhibits better electrocatalytic activity for the HER than complex **2**. In our case, the HER current density is in the magnitude of $mA \cdot cm^{-2}$ in the presence of the complexes, which is much larger than the values reported in the literatures.[5,7a] It is probably due to the solubilities of the complexes in aqueous solution, which can afford ion conductivities in the system. The electrocatalytic activities of the two complexes are probably not related with the unsaturated metal centers in the structures. It is expected that the reduction of H^+ is overlapped by the reduction of Mo (V) in the complexes. Complex **1** shows visible-light photochromism, which is because the Mo (VI) in complex **1** can be partially reduced to Mo (V) when irradiated by visible-light. In the presence of complex **1**, the HER current is enhanced with visible-light illumination in comparison to the current without light illumination. The detailed mechanism is under investigation.

Supporting Information

Crystallographic data; PXRD patterns; UV-vis absorption spectra; CVs; Tafel plots; TG curve and other supplementary material are included in the supporting information. This information is available free of charge via the Internet at http://pubs.rsc.org/.

Financial supports from the National Natural Science Foundation of China (No. 21371184), the Fundamental Research Funds for the Central Universities (No. CQDXWL-2012-024) and Chongqing Key Laboratory of Chemical Process for Clean Energy and Resource Utilization are gratefully acknowledged.

References

1 (a) M. Grätzel, *Acc. Chem. Res*., 1981, **14**, 376; (b) A. J. Brad and M. A. Fox, *Acc. Chem. Res.*, 1995, **28**, 141; (c) T. R. Cook, D. K. Dogutan, S. Y. Reece, Y. Surendranath, T. S. Teets and D. G. Nocera, *Chem. Rev.*, 2010, **110**, 6474.

2 (a) A. J. Esswein and D. G. Nocera, *Chem. Rev.*, 2007, **107**, 4022; (b) M. R. DuBois and D. L. DuBois, *Chem. Soc. Rev*., 2009, **38**, 62; (c) F. Gloaguen and T. B. Rauchfuss, *Chem. Soc. Rev.*, 2009, **38**, 100.

3 (a) B. Nepal and S. Das, *Angew. Chem. Int. Ed*., 2013, **52**, 7224; (b) J. C. Fontecilla-Camps, A. Volbeda, C. Cavazza and Y. Nicolet, *Chem. Rev.*, 2007, **107**, 4273; (c) D. Merki, H. Vrubel, L. Rovelli, S. Fierro and X. L. Hu, *Chem. Sci.*, 2012, **3**, 2515; (d) A. M. Appel, S. J. Lee, J. A. Franz, D. L. DuBois and M. R. DuBois, *J. Am. Chem. Soc.*, 2009, **131**, 5224.

4 (a) J. F. Capon, F. Gloaguen, F. Y. Pétillon, P. Schollhammer and J. Talarmin, *Coord. Chem. Rev*., 2009, **253**, 1476; (b) S. Losse, J. G. Vos and S. Rau, *Coord. Chem. Rev.*, 2010, **254**, 2492; (c) V. Artero, M. Chavarot-Kerlidou and M. Fontecave, *Angew. Chem., Int. Ed.*, 2011, **50**, 7238; (d) M. R. DuBois and D. L. DuBois, *Acc. Chem. Res.*, 2009, **42**, 1974.

5 (a) Y. Gong**,** T. Wu, P. G. Jiang, J. H. Lin and Y. X. Yang, *Inorg. Chem.,* 2013, **52**, 777; (b) Y. Gong, Z. Hao, H. F. Shi, P. G. Jiang, M. M. Zhang and J. H. Lin, *ChemPlusChem*, 2014, **79**, 266; (c) Y. Gong, H. F. Shi, Z. Hao, W. Hua and J. H. Lin, *Cryst. Growth Des.,* 2014, **14**, 649; (d) Y. Gong, H. F. Shi, Z. Hao, J. L. Sun and J. H. Lin, *Dalton Trans*., 2013, **42** 12252.

6 (a) A. Dolbecq, E. Dumas, C. R. Mayer and P. Mialane, *Chem. Rev.,* 2010, **110**, 6009; (b) S. T. Zheng, J. Zhang, X. X. Li, W. H. Fang and G. Y. Yang, *J. Am. Chem. Soc.,* 2010, **132**, 15102; (c) A. K. Cuentas-Gallegos, M. Lira-Cantú, N. Casañ-Pastor and P. Gómez-Romero, *Adv. Funct. Mater.,* 2005, **15**, 1125; (d) R. M. Yu, X. F. Kuang, X. Y. Wu, C. Z. Lu and J. P. Donahue, *Coordin. Chem. Rev.,* 2009, **253**, 2872; (e) J. W. Han and C. L. Hill, *J. Am. Chem. Soc.,* 2007, **129**, 15094; (f) H. N. Miras, J. Yan, D. L. Long and L. Cronin, *Chem. Soc. Rev.*, 2012, **41**, 7403; (g) H. Y. An, E. B. Wang, D. R. Xiao, Y. G. Li, Z. M. Su and L. Xu, *Angew. Chem. Int. Ed*., 2006, **45**, 904.

7 (a) B. Nohra, H. E. Moll, L. M. R. Albelo, P. Mialane, J. Marrot, C. M. Draznieks, M. O'Keeffe, R. N. Biboum, J. Lemaire, B. Keita, L. Nadjo and A. Dolbecq, *J. Am. Chem. Soc.*, 2011, **133**, 13363; (b) L. Yang, S. Kinoshita, T. Yamada, S. Kanda, H. Kitagawa, M. Tokunaga, T. Ishimoto, T. Ogura, R. Nagumo, A. Miyamoto, and M. Koyama, *Angew. Chem., Int. Ed.*, 2010, **49**, 5348.

8 V. Niraimathi, V. Vaidhyalingam, A. Aruna and A. Vadivelu, *Acta Cienc. Indica, Chem.,* 2009, **35**, 43.

9 (a) G. M. Sheldrick, *SHELXS 97, Program for Crystal Structure Solution*, University of Göttingen, Göttingen, Germany, 1997; (b) G. M. Sheldrick, *SHELXL 97, Program for Crystal Structure Refinement*, University of Göttingen, Göttingen, Germany, 1997.

10 N. E. Brese and M. O'keeffe, *Acta Cryst.*, 1991, **B47**, 192.

11 (a) R. Xi, B. Wang, K. Isobe, T. Nishioka, K. Toriumi and Y. Ozawa, *Inorg. Chem.,*1994, **33**, 833; (b) L. D. Chen, Y. H. Wang, C. W. Hu, L. Y. Feng, E. B. Wang, N. H. Hu and H. Q. Jia, *J. Solid State Chem.*, 2001, **161**, 173.

12 (a) S. Ohkoshi, H. Tokoro, T. Hozumi, Y. Zhang, K. Hashimoto, C. Mathonière, I. Bord, G. Rombaut, M. Verelst, C. C. Moulin and F. Villain, *J. Am. Chem. Soc.,* 2006, **128**, 270; (b) D. D. Censo, S. Fantacci, F. D. Angelis, C. Klein, N. Evans, K. Kalyanasundaram, H. J. Bolink, M. Grätzel and M. K. Nazeeruddin, *Inorg. Chem*., 2008, **47**, 980.

13 Zhang J., Li W., Wu C., Li B., Zhang J. and Wu L. X., *Chem. Eur. J.*, 2013, **19**, 8129.

14 (a) A. K. Paul, G. Madras and S. Natarajan, *Phys. Chem. Chem. Phys.*, 2009, **11**, 11285; (b) G. S. Yang, H. Y. Zang, Y. Q. Lan, X. L. Wang, C. J. Jiang, Z. M. Su and L. D. Zhu, *CrystEngComm,* 2011, **13**, 1461.

15 (a) M. Alvaro, E. Carbonell, B. Ferrer, F. X. Llabrés i Xamena and H. Garcia, *Chem. Eur. J.*, 2007, **13**, 5106; (b) Z. L. Liao, G. D. Li, M. H. Bi and J. S. Chen, *Inorg. Chem.*, 2008, **47**, 4844; (c) Z. T. Yu, Z. L. Liao, Y. S. Jiang, G. H. Li, J. S. Chen, *Chem. Eur. J.*, 2005, **11**, 2642; (d) H. S. Lin and P. A. Maggard, *Inorg. Chem.*, 2008, **47**, 8044.

16 (a) M. T. Pope, Heteropoly and Isopoly Oxometalates, Springer-Verlag, Heidelberg, 1983; (b) T. R. Zhang, W. Feng, Y. Q. Fu, R. Lu, C. Y. Bao, X. T. Zhang, B. Zhao, C. Q. Sun, T. J. Li, Y. Y. Zhao and J. N. Yao, J. Mater. Chem., 2002, **12**, 1453; (c) Z. B. Han, E. B. Wang, G. Y. Luan, Y. G. Li, H. Zhang, Y. B. Duan, C. W. Hu and N. H. Hu, J. Mater. Chem., 2002, **12**, 1169; (d) Z. L. Wang, R. L. Zhang, Y. Ma, L. Zheng, A. Peng, H. B. Fua and J. N. Yao, *J. Mater. Chem.*, 2010, **20**, 1107; (e) P. Mialane, G. J. Zhang, I. M. Mbomekalle, P. Yu, J.-D. Compain, A. Dolbecq, J. Marrot, F. Sécheresse, B. Keita and L. Nadjo, *Chem. Eur. J.*, 2010, **16**, 5572.

17 L. M. Rodriguez-Albelo, A. Rabdel Ruiz-Salvador, A. Sampieri, D. W. Lewis, A. Gómez, B. Nohra, P. Mialane, J. Marrot, F. Sécheresse, C. Mellot-Draznieks, R. Ngo-Biboum, B. Keita, L. Nadjo and A. Dolbecq, *J. Am. Chem. Soc*., 2009, **131**, 16078.

18 (a) L. Cheng, X. M. Zhang, X. D. Xi and S. J . Dong, *J. Electroanal. Chem.*, 1996, **407**, 97; (b) X. L. Wang, C. Qin, E. B. Wang, Z. M. Su, Y. G. Li and L. Xu, *Angew. Chem. Int. Ed.*, 2006, **45**, 7411; (c) L. F. Yang, S. Kinoshita, T. Yamada, S. Kanda, H. Kitagawa, M. Tokunaga, T. Ishimoto, T. Ogura, R. Nagumo, A. Miyamoto and M. Koyama, *Angew. Chem. Int. Ed*., 2010, **49**, 5348; (d) X. L. Wang, H. L. Hu, G. C. Liu, H. Y. Lin and A. X. Tian, *Chem. Commun*., 2010, **46**, 6485.

19 Y. Gao and B. Wu, *Electrochemical Basis*, Chemical industry press, Beijing, **2003**, 53.

20 (a) M. Hunsom, *Spectrosc. Prop. Inorg. Organomet. Compd.,* 2012, **42**, 196; (b) S. A. Mamuru, K. I. Ozoemena, T. Fukuda and N. Kobayashi, *J. Mater. Chem*., 2010, **20**, 10705; (c) S. Ghosh, R. K. Sahu and C. R. Raj, *J. Mater. Chem*., 2011, **21**, 11973; (d) M. K. Datta, K. Kadakia, O. I. Velikokhatnyi, P. H. Jampani, S. J. Chung, J. A. Poston, A. Manivannan and P. N. Kumta, *J. Mater. Chem. A,* 2013, **1**, 4026; (e) R. N. Reddy and R. G. Reddy, *J. Power Sources,* 2004, **132**, 315.

21 M. T. M. Koper and E. Bouwman, *Angew. Chem. Int. Ed.*, 2010, **49**, 3723.

Table 2 Distances (Å) and angles (°) of the selected hydrogen bonds in complexes **1** and **2**

D	H	A	D···A distance	H···A distance	∠D–H···A
Complex **1**					
N2	H2	N8#1	2.975	2.142	163
N3	H3	O8#2	2.704	1.866	164
N6	H6	O5#3	2.861	2.192	134
N7	H7	O6#4	3.028	2.361	135
N7	H7	O4#3	3.146	2.542	128
N12	H12	O1#2	2.747	1.901	167
Complex **2**					
N5	H5	O12	2.947	2.150	154
N12	H12	O2#3	2.859	2.005	172
N12	H12	O5#3	2.865	2.418	113

Symmetry transformations used to generate the equivalent atoms:
#1: x+1/2, -y+3/2, z+1/2; #2: -x+3/2, y+1/2, -z+3/2; #3: -x+1, -y+1, -z+1; #4: x-1/2, y+1/2, z

Table 3 The centroid-centroid (CC) distance (Å) and perpendicular (P) distance (Å) involving π···π stacking interactions for complexes **1** and **2**

Plane	Plane	CC distance	P distance
*Complex **1***			
N1/N2/C1-C3	N12/C16-C20	3.975 (5)	3.512 (3)
N3-N5/C4/C5	N12/C16-C20	3.832 (5)	3.278 (3)
N7/N8/C11-C13	N9A-N11A/C14A/C15A	4.027 (5)	3.371 (4)
N7/N8/C11-C13	N12A/C16A-C20A	3.832 (5)	3.278 (3)
*Complex **2***			
Co1/N1/N6/C2/C3	N1B-N3B/C1B/C2B	3.936 (6)	3.282 (2)
Co1/N8/N13/C11/C12	Co1A/N8A/N13A/C11A/C12A	3.536 (6)	3.224 (4)
Co1/N8/N13/C11/C12	N1B-N3B/C1B/C2B	3.593 (5)	3.334 (4)
Co1/N8/N13/C11/C12	N8A-N10A/C10A/C11A	3.274 (6)	3.228 (4)
N4-N6/C3/C4	N7D/C5D-C9D	3.666 (5)	3.217 (3)
N8-N10/C10/C11	N11A-N13A/C12A/C13A	3.719 (6)	3.202 (4)
N8-N10/C10/C11	N7B/C5B-C9B	3.796 (6)	3.289 (4)

Symmetry transformations used to generate equivalent atoms:
A 1-*x*, 2-*y*, 1-*z* B 1-x, 1-y, 1-z D -x, 1-y, 1-z